TYPE Original Research
PUBLISHED 19 November 2025
DOI 10.3389/feart.2025.1674441



OPEN ACCESS

EDITED BY
Wenling Tian,
China University of Mining and
Technology, China

REVIEWED BY Mohammad Azarafza, University of Tabriz, Iran Youssef Bammou, Cadi Ayyad University, Morocco

*CORRESPONDENCE
Wanjia Guo,

■ 121752646@qq.com
Meiben Gao,
■ 578209337@qq.com

RECEIVED 28 July 2025
REVISED 25 October 2025
ACCEPTED 30 October 2025
PUBLISHED 19 November 2025

CITATION

Wang L, Guo W, Bai S, Bian R, Zhang L, He Z, He B, Chen F, Jing J and Gao M (2025) Landslide deformation mechanism and stability analysis under earthquake and rainfall conditions: a case study of Shibanping landslide.

Front. Earth Sci. 13:1674441. doi: 10.3389/feart.2025.1674441

COPYRIGHT

© 2025 Wang, Guo, Bai, Bian, Zhang, He, He, Chen, Jing and Gao. This is an open-access article distributed under the terms of the Creative Commons Attribution License (CC BY). The use, distribution or reproduction in other forums is permitted, provided the original author(s) and the copyright owner(s) are credited and that the original publication in this journal is cited, in accordance with accepted academic practice. No use, distribution or reproduction is permitted which does not comply with these terms.

Landslide deformation mechanism and stability analysis under earthquake and rainfall conditions: a case study of Shibanping landslide

Lijuan Wang^{1,2,3}, Wanjia Guo^{1,2}*, Shiming Bai⁴, Rui Bian^{1,2}, Liang Zhang⁴, Zhihao He^{1,2,3,4}, Binbin He³, Fujiang Chen⁴, Juncheng Jing⁵ and Meiben Gao^{1,2,3,4,6}*

¹Sichuan Academy of Safety Science and Technology, Chengdu, Sichuan, China, ²Major Hazard Measurement and Control Key Laboratory of Sichuan Province, Chengdu, China, ³School of Resources and Environment, University of Electronic Science and Technology of China, Chengdu, Sichuan, China, ⁴School of Emergency Management, Xihua University, Chengdu, Sichuan, China, ⁵Chongqing 208 Geological Environment Research Institute Co., Ltd., Beibei, China, ⁶Key Laboratory of Landslide Risk Early-Warning and Control, Ministry of Emergency Management, Chengdu University of Technology, Chengdu, China

Landslides, as a common geological disaster, pose a significant threat to the safety of people's lives and property, as well as the stability of infrastructure in mountainous areas. Based on a detailed investigation of the Shibanping landslide, this paper first analyzes the causes and mechanisms of the landslide. Secondly, the plane sliding method and numerical simulation method are adopted to explore the changes in the stability of the landslide under natural, rainfall, and seismic conditions. The research results show that the instability of the Shibanping landslide is closely related to the complex geological structure, topography, geomorphology, lithology, excavation activities, hydrological changes caused by rainfall, and seismic effects in the area. The deformation of the landslide starts with tensile cracking and downward displacement at the top. Then, it gradually expands to the deep layer and the front edge under the influence of rainfall and excavation; its mechanism is progressive-bedding slip. Rainfall increases the self-weight, saturation, and pore water pressure of the rock and soil mass, leading to a continuous decrease in effective stress, thereby exacerbating the instability of the landslide. Earthquakes reduce the stability of the slope through shear stress caused by seismic waves. The stability calculation results indicate that the landslide has a certain degree of stability under natural conditions, but its stability decreases significantly when rainfall or earthquakes occur. This study provides theoretical support for the analysis and prevention of landslide stability, and is of great significance especially for the prediction, prevention, and control of landslides in areas with long-term rainfall and high earthquake frequency.

KEYWORDS

landslide, mechanism, rainfall, earthquake, numerical simulation

1 Introduction

As a common geological hazard, landslides pose a severe threat to the safety of people's lives and property as well as the stability of infrastructure. The occurrence of landslides is not only closely related to natural factors but also tightly linked to external environmental conditions such as earthquakes and rainfall (Zhu et al., 2013; Marui and Wanfg, 2015; Montoya-Araque et al., 2025). Especially in recent years, with the frequent occurrence of earthquakes and the prevalence of extreme weather, it not only directly affects the safety of various structures and infrastructure (Qiu et al., 2023; He et al., 2023; Rajaram et al., 2025; Tang and Marshall, 2025) but also significantly increases the probability of landslide occurrences. A large number of landslides are induced under the influence of earthquakes and rainfall (Sassa et al., 2023; Wu et al., 2023; Chen et al., 2024; Song et al., 2025). According to statistics, the number of deaths caused by landslides worldwide exceeds 10,000 each year, and the direct economic losses amount to billions of US dollars (Zhu et al., 2013; Marui and Wanfg, 2015). Therefore, it has become particularly important to study the genetic mechanisms and stability of landslides under earthquake and rainfall conditions.

The mechanism of landslides is complex and closely related to the combined effects of factors such as rock mass properties, topography, geomorphology, precipitation, and earthquakes (Iverson, 2000; Nanehkaran et al., 2021; Moska et al., 2024). Studies have shown that the relationship between rainfall and landslides is significant. The precipitation increases the pore water pressure of the rock mass and weakens the shear strength of the rock mass, thereby accelerating the occurrence of landslides (Montgomery and Dietrich, 1994; Gao et al., 2025). The impact of rainfall is not limited to the rise of water level; it also further reduces the stability of slopes by increasing soil saturation (Marotti et al., 2023). During an earthquake, the rock mass is subjected to seismic loads, and the increase in its shear stress also promotes the sliding of unstable slopes (Khan and Wang, 2021; Nandi and Ghosh, 2025). Although existing research on landslide mechanisms has made certain progress, there are still many unsolved problems in the accurate assessment of landslide stability and safety under rainfall and earthquake conditions (Nanehkaran et al., 2022; Cemiloglu et al., 2023). Studying the mechanism of landslides is crucial for in-depth understanding of the impact of rainfall and earthquakes on landslides. Rainfall can significantly affect slope stability by changing soil moisture content, increasing pore water pressure, and altering the mechanical properties of rock and soil (Ma et al., 2025; Wang et al., 2025). Earthquakes, on the other hand, directly affect the stability of landslide masses through the shear stress generated by seismic wave propagation and their vibration effect on rock masses (Ren et al., 2023). Especially in the scenario where rainfall and earthquakes occur alternately, the synergistic effect of the two makes the mechanism of landslide occurrence more complex. Therefore, revealing the genetic mechanism of landslides under this combined factor has important academic significance and practical value.

Although there have been some studies on landslide stability analysis (Kurlenya et al., 2016; Mao et al., 2023), most of these studies focus on the impact of a single factor, primarily concentrating on the effect of either rainfall or earthquakes on

landslides. Research on landslide stability under the simultaneous action of rainfall and earthquakes still lacks comprehensive and in-depth exploration (Li et al., 2023), especially regarding the dynamic changes of landslides under complex rainfall and seismic conditions. Current landslide stability analyses are mostly based on static conditions, failing to fully consider the time effect and the impact of alternating long-term rainfall and earthquakes. Therefore, more detailed research is urgently needed.

In recent years, research on landslide stability under rainfall and seismic conditions has gradually increased. Through field observations, numerical simulations, and machine learning methods (Nanehkaran et al., 2023), many scholars have studied the deformation behavior and the stability of landslide under different rainfall durations and intensities (Shu et al., 2024; Zhao et al., 2025). The impact of seismic loads on landslides has also received widespread attention; in particular, studies based on large-scale seismic data and post-earthquake landslide events have revealed the triggering effect of earthquakes on slope instability (Montoya-Araque et al., 2025; Song et al., 2025). These studies not only help to understand the internal mechanism of landslide occurrence but also provide a theoretical basis for landslide prevention and control. Although existing research has provided partial theoretical support for landslide prevention and control, there are still the following research gaps. First, the analysis of landslide stability lacks in-depth research on the effects of rainfall and earthquakes, especially the changes in landslide stability when the two act alternately or simultaneously. Second, existing research is mainly based on short-term rainfall and post-earthquake landslide observations, and lacks analysis of landslide evolution under long-term rainfall and seismic activity conditions. Therefore, comprehensive research on changes in landslide stability under long-term rainfall and seismic conditions is urgently needed.

This study aims to explore the deformation characteristics of the landslide mass and reveal the causes and mechanisms of the landslide through a detailed investigation of the Shibanping landslide. It will focus on analyzing the deformation and stability changes of the landslide under rainfall and seismic conditions, providing key data support for subsequent landslide safety analysis. Adopting a combined method of field investigation and numerical simulation, this study first conducts a field investigation of the Shibanping landslide to identify the landslide's deformation characteristics, sliding bed features, and potential sliding surface properties. Based on these investigation data, combined with numerical simulation software, the study analyzes the stability changes of the landslide under the action of rainfall and earthquakes, explores the causes and mechanisms of the landslide, and calculates the safety factor of the landslide under different conditions.

The research results will reveal the variation laws of landslide stability and safety under rainfall and seismic conditions. By indepth analyzing the deformation and stability of the landslide in complex environments, this study provides reliable mechanical parameters and a theoretical basis for the prevention and control of landslide disasters in areas with long-term rainfall and high earthquake frequency.

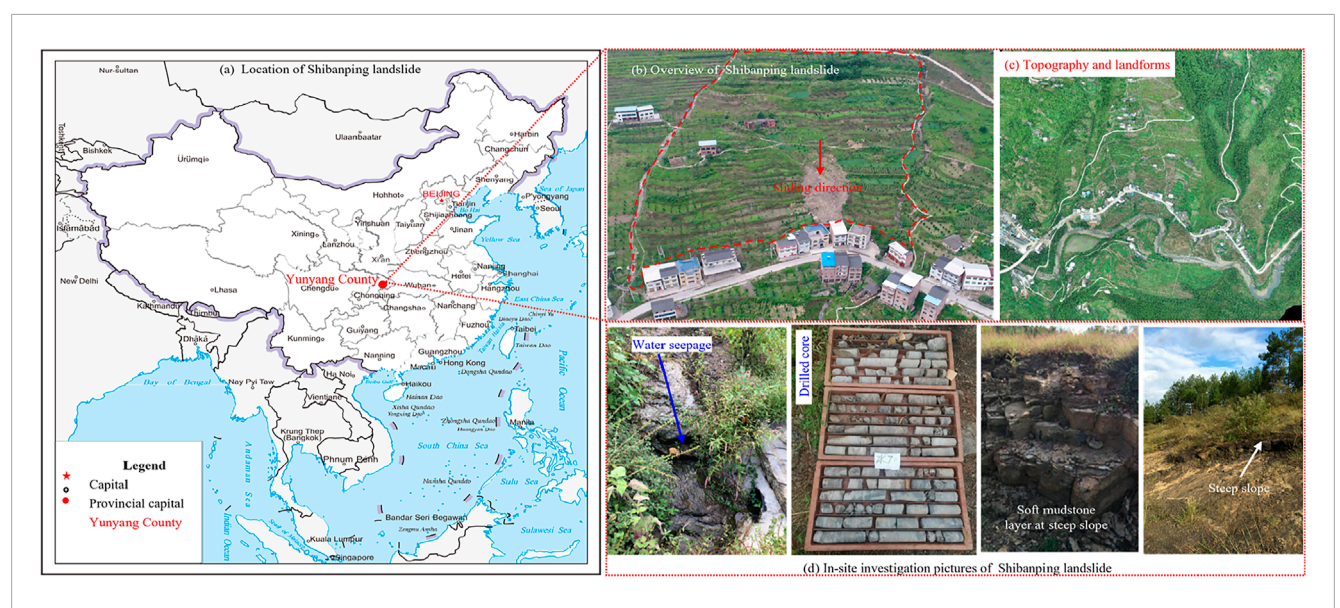


FIGURE 1
Location and engineering geological conditions of Shibanping landslide (Modified by Gao et al., 2025). (a) Location of Shibanping landslide. (b)
Overview of Shibanping landslide. (c) Topography and landforms. (d) In-site investigation pictures of Shibanping landslide.

2 Engineering geological conditions of Shibanping slope

The Shibanping landslide is situated in Group 15, Zhongyuan Village, Longtang Community, Ping'an Town, Yunyang County, Chongqing Municipality, with geographical coordinates of 108.451697° E longitude and 31.0003° N latitude. It is located at the border of Wanzhou District and Yunyang County, where transportation is convenient—the distance to Yunyang County is approximately 30 km (Figure 1a). Yunyang County belongs to the subtropical warm and humid monsoon climate zone, with an annual average temperature of 18.7 °C and a multi-year average precipitation of 1,145.1 mm. There is a small river gully on the northern side of the landslide, and its water level is subject to seasonal control: the water level is generally 402.00 m during the dry season and 406.2 m during the flood season.

The landslide is located on the northern limb of the Tiefengshan Anticline, with an overall terrain sloping from high in the south to low in the north, belonging to a structural denudation low-mountain single slope geomorphic area. The topographic slope is roughly 15°–25°, presenting a single-faced slope shape. There are multiple stepped small rocky steep banks on the slope; these steep banks are free-faced (exposed to the air) and generally 1–3 m high (Figures 1b,c).

Geological survey results show that the strata exposed in the landslide area, from the youngest to the oldest, are the Holocene silty clay of the Quaternary System ($Q_4^{\text{el+dl}}$), colluvial-deluvial layer ($Q_4^{\text{col+dl}}$), and Lower Jurassic Ziliujing Formation ($J_{1-2}z$) (Figure 1d). The rock strata occur in a monocline, with an attitude of 355° \angle 15° and little variation in dip angle. The lithology mainly includes sandstone, argillaceous sandstone, and argillized interlayers. The argillized interlayers are mainly distributed at the contact zones of rock strata, showing an argillaceous structure, with phenomena of water erosion, rusting, and argillization. They have

low strength and discontinuous distribution, serving as potential sliding surfaces for unstable slopes. The seismic fortification intensity in the area is Degree VI, with a peak ground acceleration of 0.05 g and a characteristic period of the ground motion response spectrum of 0.35 s. The groundwater in the landslide area is mainly recharged by atmospheric rainfall, and the groundwater types are mainly pore water in Quaternary unconsolidated rocks and bedrock fissure water. There is little groundwater in the landslide mass; however, during heavy rain, the landslide is recharged by infiltration from the deformed body of the gully on the right side, and water seeps out from most of the free faces at the front edge of the free-sliding area.

The land use in this area is mainly dry farmland, and the surface of the mountain at the upper part of the landslide is covered with relatively abundant vegetation. Human engineering activities mainly include house construction and road cutting for village highways, which have formed artificial slopes with a height of 3–6 m.

3 Deformation characteristics and formation mechanism of Shibanping landslide

3.1 Deformation characteristics

The landslide is bounded by gullies on the east and west sides, by a village road at the rear edge, and by houses inside the highway at the front edge (Figure 2a). The landslide has a longitudinal length of approximately 157 m, a transverse width of about 65 m, and a tongue-like planar shape. It has an average thickness of around 4.0 m, a distribution elevation ranging from 473 m to 431 m, an area of approximately 1.78×10^4 m², and a volume of about 7.12 \times 10^4 m³. The main deformation and failure characteristic of the landslide is the collapse of the landslide's free face. The potential



sliding direction of the landslide is 355° , and the height of the dip-slope (consistent with the rock stratum dip direction) with a free face is 3-6 m.

Based on field investigations, after the continuous extremely heavy rainfall in August 2014, the Shibanping landslide exhibited deformation phenomena such as ground tensile cracking and local downward displacement (Figure 2a, CR1~CR2 & COL1). These deformation cracks continued to expand and extend slowly after continuous rainfall or heavy rain every year. The overall deformation signs of the landslide were mainly concentrated in the rear part. On 30 June 2020, the excavation for village road construction

induced multiple rocky cracks (Figure 2a, CR3~CR7), and the slope underwent deformation and failure along the rock bedding planes. On 25 July 2020, multiple deformation and collapse events occurred in the front part of the unstable slope (Figure 2a, COL2~COL3). A small-scale shallow rocky landslide also occurred: the landslide area was approximately 30 m in length, 15 m in width, 3 m in thickness, and about 450 m³ in volume.

According to the field exploration results: Weak mudstone layers can be seen at local steep slopes on the surface (Figure 2b left). Exploratory wells (TJ1) and boreholes have revealed the presence of weak zones and a small number of argillized interlayers

in the landslide area (Figure 2b middle and right). Among the 24 boreholes, one borehole shows signs of water erosion and argillization (Figure 2b right), with a thickness of 0.10–0.30 m. It is inferred that the potential sliding surface is the interface of the argillized interlayer; the sliding surface is in a planar straight-line shape, with a depth ranging from 6.5 m to 15.2 m.

3.2 Formation mechanism analysis

3.2.1 Formation causes

3.2.1.1 Topography and landforms

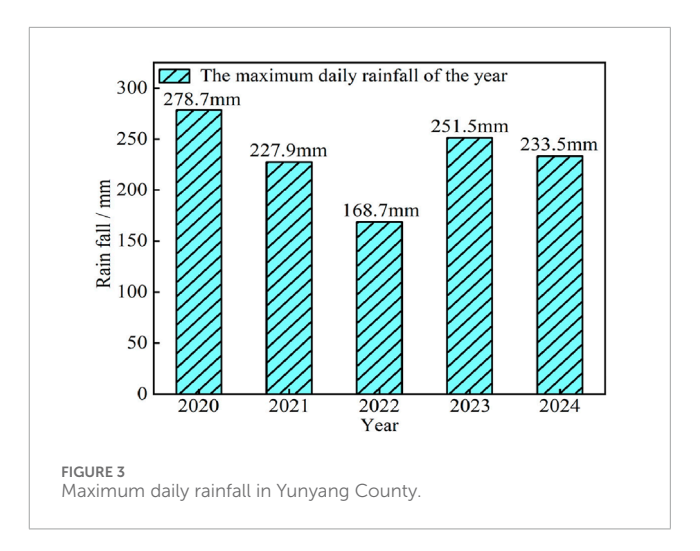
The landslide area is located in the tectonically eroded low mountain landform zone, with an overall topography that slopes from high to low towards the north. The topographic relief is considerable. The steep slopes, particularly those with a gradient ranging from 15° to 25°, are a major factor contributing to the landslide's occurrence. Except for the residential areas, where the topography is relatively gentle, the slope generally has gradients between 15° and 25°, and the slope exhibits localized outward-facing steep features. Specifically, at the front edge of the slope, the construction of the highway and houses has significantly developed the free face, reaching a height of 6 meters, which provides spatial conditions for landslide formation. These topographic features contribute to the poor stability of the slope, especially under external disturbances such as rainfall and earthquakes, making the slope more prone to instability.

Several steep, bedrock-capped cliffs, with heights ranging from 1 to 3 meters, exist on the slope. The presence of these cliffs results in significant topographic changes and causes the gravitational forces on the slope to concentrate in localized areas, further promoting the occurrence of the landslide. The steep slopes and outward-facing structures enhance stress concentration within the slope, thereby creating favorable conditions for landslide initiation.

3.2.1.2 Geological structure and stratigraphic lithology

The landslide area is located on the northwest limb of the Tiefengshan anticline. The bedding strikes at 355° and dips between 10° and 20°, with the dip direction consistent with the slope direction, forming a geologic structure conducive to sliding. Two major structural fractures in the unstable slope area are arranged in an "X" pattern. One set of fractures dips between 25° and 40° with an intersection angle of 81°–84°, while the other set dips between 260° and 282°, with an intersection angle of 83°–88°. The presence and intersection of these fractures provide favorable conditions for landslide initiation, particularly for deformation and cracking along the rear edge of the landslide. These fractures make the rock mass more susceptible to slippage along the fractures when subjected to external forces such as rainfall or seismic activity, thus decreasing the overall stability of the slope.

In terms of stratigraphy, the landslide area is mainly composed of sandstone, mudstone sandstone, and clay-rich interlayers. This combination of rock types forms a stratigraphic profile characterized by hard upper layers, a middle section with weak interlayers, and a relatively impermeable layer at the base. This lithological combination is a key factor in the landslide's instability. The clay-rich interlayers, as the primary weak links in the sliding



surface, have low shear strength, and under the influence of rainfall or seismic events, they are prone to shear failure, leading to the initiation of the landslide. Furthermore, the mechanical property differences between mudstone sandstone and sandstone increase stress concentration between layers, further enhancing the likelihood of a landslide.

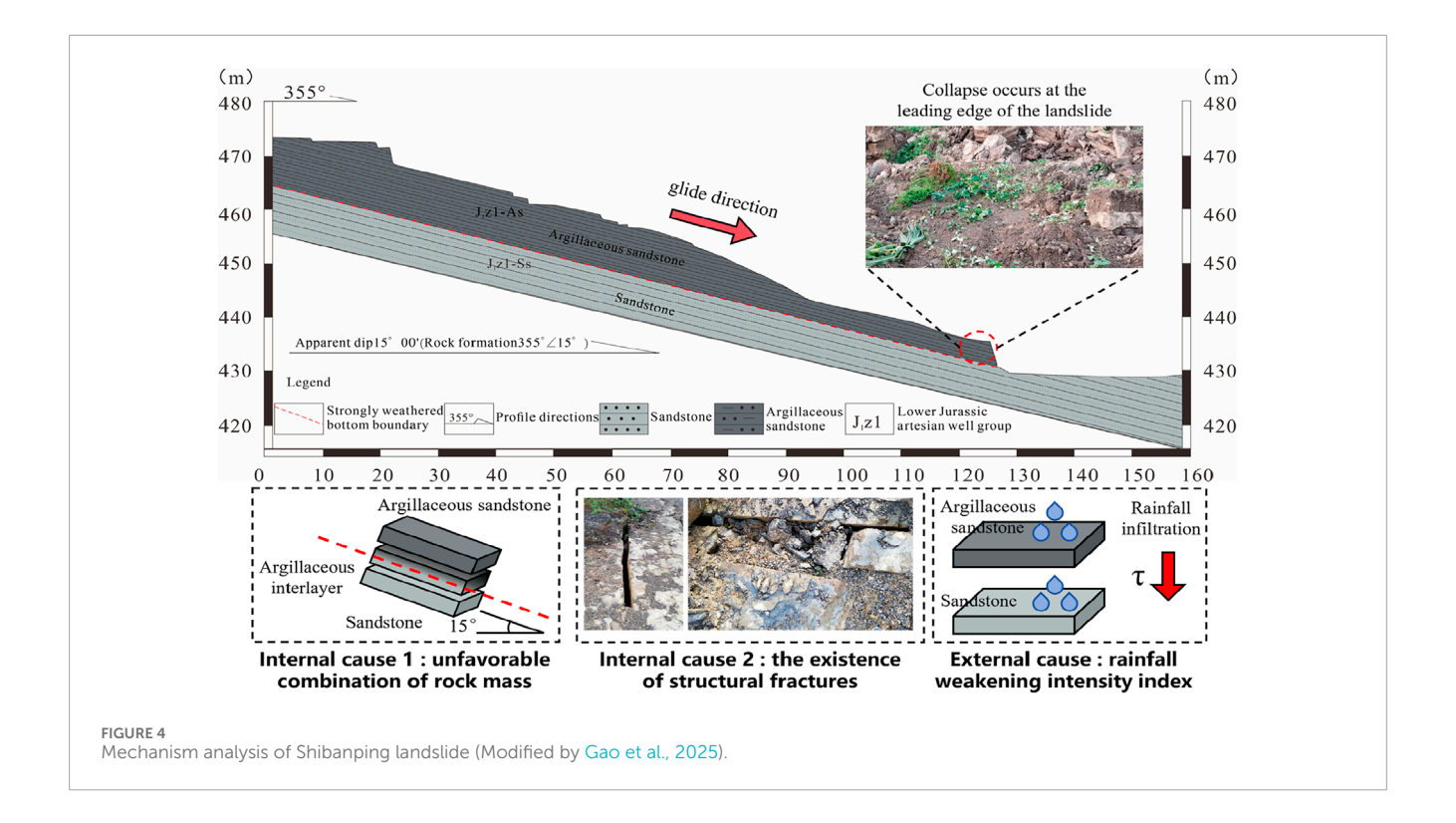
3.2.1.3 Meteorological and hydrological conditions

Yunyang County experiences abundant rainfall, particularly between May and October, with frequent heavy rainstorms. According to statistical data, the maximum daily precipitation can reach 278.7 mm (Figure 3). The soil in the landslide area is primarily composed of sandstone and rubble, which have relatively good permeability. Continuous and concentrated rainfall plays a significant role in triggering instability in the slope. As rainfall infiltrates the surface and permeates through structural fractures, water enters the clay-rich interlayers and reduces their shear strength, weakening the sliding surface in this area. Moreover, the dynamic water pressure generated during infiltration further weakens the stability of the landslide body and increases the risk of sliding.

Rainfall infiltrates and reduces the strength of the clay-rich interlayers, which further decreases the shear strength of the potential sliding surface. The cumulative effects of precipitation and water infiltration make the sliding surface more susceptible to shear failure, which eventually leads to deformation and failure of the landslide body. The variation in meteorological and hydrological conditions (such as the intensity and duration of heavy rainfall) plays a decisive role in the triggering and evolution of the landslide, especially in this region, where the frequency and intensity of rainfall are high, making rainfall the primary trigger for landslide occurrence.

3.2.2 Mechanism analysis

The sliding mechanism of the Shibanping landslide is a complex physical process influenced by multiple factors. Based on the topographical features and causation analysis, the landslide exhibits a relatively gentle slope with an overall single-sided slope shape, a thin soil layer, and extensive exposure of the bedrock. The deformation and failure of the landslide primarily involve



localized slip-like deformation along the free face (Figure 4). This sliding pattern is closely related to the geological structure, lithological combination, and external disturbance factors affecting the slope.

The local topography of the landslide area is relatively steep, particularly at the front edge, where significant free-facing structures have formed, providing spatial conditions for landslide initiation. In the rear edge and on both sides of the landslide, the geological structure is complex due to the intersection of two sets of structural fractures. Specifically, the lithological profile consists of hard upper layers, weak interlayers in the middle, and relatively impermeable layers at the base. This lithological combination creates clear weak surfaces, particularly in the middle clay-rich interlayers and mudstone layers, which are key factors in the landslide's occurrence.

The bedrock overlying the slope is primarily composed of sandstone and shell sandstone, which exhibit relatively high permeability. Rainfall-induced water infiltration intensifies the hydrological effect of the fractures, allowing water to infiltrate into the rock mass, particularly into the softer clay-rich sandstones and mudstone interlayers. The shear strength of these weaker layers decreases significantly under the influence of water infiltration, leading to the gradual formation and expansion of the potential sliding surface. As water infiltration continues, the physical and mechanical properties of the weaker interlayers change, causing a significant reduction in the strength of the rock mass, thus facilitating the deformation of the slope along the bedding planes.

Under the influence of external disturbances such as rainfall, the deformation of the slope gradually accumulates. Over time, stress concentrates on the weak surfaces, which further accelerates the sliding of the landslide body. The gravitational forces exacerbate the deformation process along the bedding planes, particularly at the junctions of fractures and clay-rich interlayers, where deformation extends deeper into the rock mass, ultimately leading to the formation of the landslide. The long-term accumulation of deformation makes the stress concentration more pronounced, eventually overwhelming the shear strength of the rock mass and resulting in the initiation of the landslide.

In summary, the sliding mechanism of the Shibanping landslide is shaped by an interplay of factors including topography, lithology, rainfall infiltration, and long-term deformation accumulation. The hard lithology of the slope and the presence of permeable layers contribute to the significant effect of rainfall infiltration on the weak interlayers. Together with the effects of long-term deformation and gravitational forces, the sliding surface of the slope gradually forms, ultimately leading to the landslide. In 2014, under rainfall conditions, tensile cracking and downward displacement first occurred at the top of the landslide. As rainfall infiltrated along the cracks, the argillized interlayers were softened. The anti-sliding force of the upper part of the landslide gradually decreased, while the transmitted sliding force continued to increase. Meanwhile, the lower part of the landslide experienced reduced antisliding force due to excavation, which further led to cracking on both sides of the landslide (Figure 2, CR3~CR7). Eventually, this caused the collapse of the landslide's front edge, particularly COL2 and COL3 in Figure 2, which exhibit bulge-like characteristics. This indicates that the front edge of the landslide, as an antisliding segment, underwent progressive destruction. At the same time, the dip direction of the rock strata was consistent with the slope direction, and shear sliding occurred along the weak layers. In summary, the mechanism of the Shibanping landslide can be considered as progressive-bedding slip.

4 Landslide stability analysis

4.1 Methods

This study intends to adopt theoretical and numerical simulation methods to analyze the stability of the Shibanping landslide. According to Figure 4 above, the landslide slides along the weak planes between rock strata, and the sliding surface is a straight line; therefore, the plane sliding method is used for theoretical analysis.

The plane sliding method is a classic approach for landslide stability analysis, which mainly assumes that the sliding surface is a single continuous plane (Figure 5a). Based on the assumption that the landslide mass slides along the argillized interlayers, this method is widely applied in the stability analysis of bedding rock landslides, featuring the advantages of simple and efficient calculation processes. Formula 1 presents its stability calculation equation.

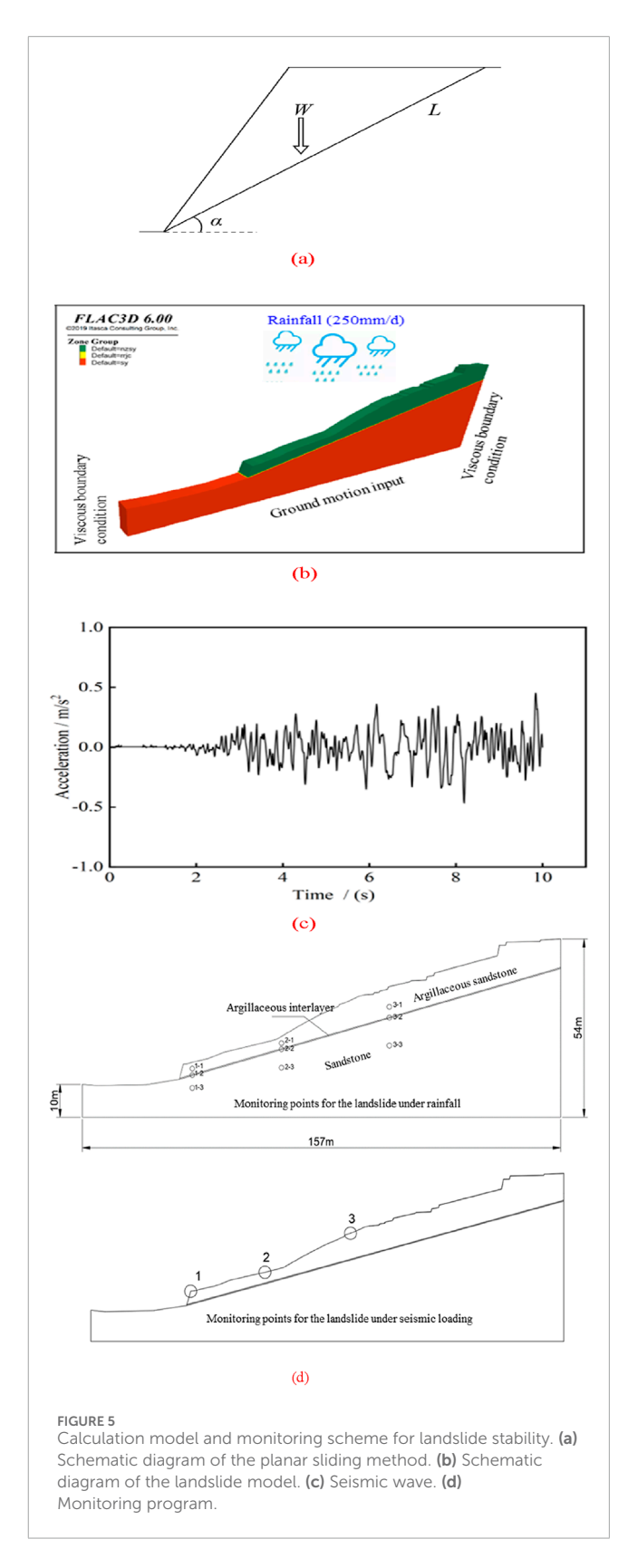
For numerical simulation, the widely used FLAC3D software is employed to analyze the stability of the landslide under natural conditions, rainfall, and seismic action. In the slope stability analysis using FLAC3D, the strength reduction method is a common technique based on the Mohr-Coulomb criterion. It simulates the process of gradual reduction in material strength until slope instability by progressively reducing the cohesion (c) and internal friction angle (ϕ) of the rock-soil mass. When the reduced numerical model exhibits continuous displacement increase, mesh distortion, or calculation non-convergence (e.g., the number of iterations exceeds the set threshold, or the unbalanced force ratio exceeds the limit), and the plastic zone penetrates the potential sliding surface, the slope is considered to reach the limit equilibrium state. At this point, the value F represents the safety factor of the landslide, also known as the stability coefficient.

$$F_{s} = \frac{(W\cos\alpha - U_{1} - U_{2}\sin\alpha - AW\sin\alpha)\tan\varphi + cL}{W\sin\alpha + U_{2}\cos\alpha + AW\cos\alpha}$$
(1)

Where F_s is the safety factor of the slope, c is the cohesion of the sliding surface, φ is the internal friction angle of the sliding surface, W is the weight of the sliding mass, L is the length of the sliding surface, U_1 is the buoyant force acting on the sliding mass from the ground, U_2 is the water pressure in the tensile cracks, and α is the inclination of the sliding surface, A is seismic acceleration.

The main sliding section was selected, and the original CAD topographic file was imported into Rhino software for meshing, with the mesh size set to 1 m. The landslide model has a length of 157 m, a width of 5 m, and a height of 54 m. Hexahedral elements were used for the model, with a total of 21,325 elements. From top to bottom, the model consists of argillaceous sandstone, argillized interlayers, and sandstone (Figure 5b).

The Mohr-Coulomb model was adopted as the constitutive model for the simulation. This model defines the shear strength of materials through the internal friction angle (ϕ) and cohesion (c), and can accurately describe the plastic yielding and failure behavior of soil or rock masses under shear action. Before conducting the simulation, it is necessary to set initial conditions and boundary conditions. Since the landslide is constrained by the surrounding slope mass in reality, boundary conditions need to be applied to the model. Therefore, the model was constrained as follows based on actual conditions: the bottom was constrained for displacement in the X and Y directions; the left and right sides were only



constrained for displacement in the X direction; the slope surface was unconstrained and treated as a free face. The initial stress was the self-weight stress acting vertically downward along the Z-axis. A fixed flow rate (250 mm/d) was applied to the slope surface to

simulate rainfall conditions (with rainfall durations of 12 h, 24 h, 36 h, 48 h, and 60 h), while the rest of the model boundaries were set as impermeable boundaries. As mentioned earlier, the seismic fortification intensity in the landslide area is Degree VI, with a peak ground acceleration of 0.05 g. For this reason, a 0.05 g PEER seismic wave (Figure 5C) was applied to the bottom of the model to simulate seismic action (with a duration of 7 s), and viscous boundary conditions were set on the left and right sides.

During the simulation, the pore water pressure, saturation, and displacement of the landslide were monitored; the monitoring points are detailed in Figure 5d. Combined with relevant literature, local empirical values, and test results (Wang, 2023; Gao et al., 2025), the calculation parameters for the stability analysis of the Shibanping landslide were comprehensively determined. The specific values for argillaceous sandstone, argillized interlayers, and sandstone are shown in Table 1 below.

4.2 Calculation results and analysis of stability

The stability calculation results of the Shibanping landslide obtained via two methods under different working conditions are presented in Table 2 and Figure 6 below.

According to Table 1, under natural conditions, the stability coefficients calculated by the plane sliding method and the numerical simulation method are 1.37 and 1.36, respectively (Figure 6a), indicating that the landslide is in a stable state under natural conditions.

Under rainfall conditions, the stability coefficient calculated by the plane sliding method is 0.99, which means the landslide is in an unstable state; in contrast, the stability coefficient obtained by the numerical simulation method is 1.03, indicating the landslide is in a basically stable state. As shown in Figure 6b, at the beginning of rainfall, the safety factor of the landslide decreases gradually with the increase of rainfall duration. It drops from 1.36 (after 12 h of rainfall) to 1.05 (after 48 h of rainfall), and the change during this period is relatively significant. However, when the rainfall duration is extended to 60 h, the safety factor of the landslide further decreases to 1.03, with a significantly reduced variation range. Compared with the safety factor at 48 h, the change becomes relatively stable. Thus, the safety factor at this point can be regarded as the stability coefficient of the landslide.

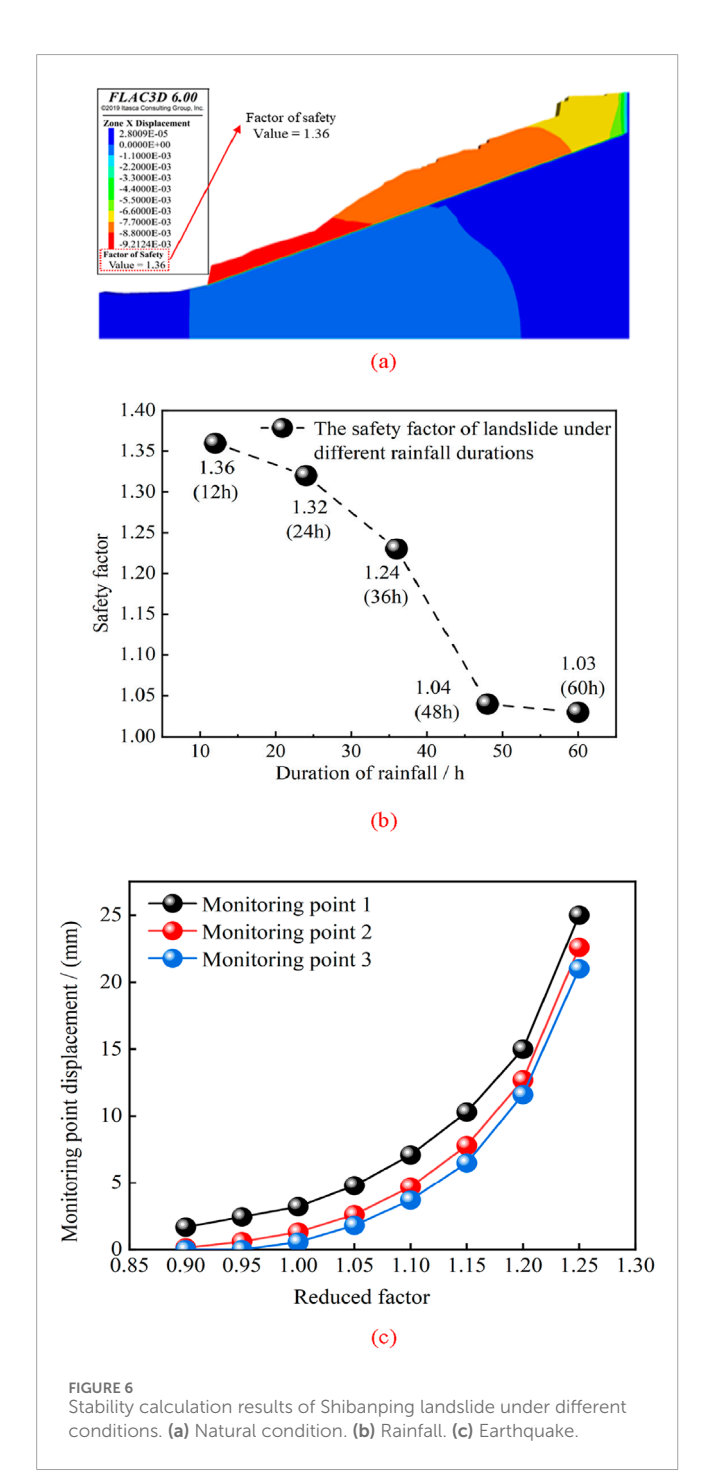
Under seismic conditions, the stability coefficients calculated by the plane sliding method and the numerical simulation method are 1.12 and 1.15, respectively, suggesting the landslide is in a basically stable state. As illustrated in Figure 6c, when the reduction coefficient reaches 1.15, the horizontal characteristic displacement of the monitoring points shows a trend of sharp increase. This phenomenon indicates that the stability of the landslide decreases rapidly, and the deformation of the landslide mass begins to intensify sharply. It can be considered that the potential sliding surface has been basically connected at this point, which means the sliding surface of the landslide is gradually expanding and tending to a continuous state. Therefore, the reduction coefficient of 1.15 can be regarded as the critical safety factor of the landslide, i.e., the stability coefficient.

TABLE 1 Stability calculation parameters of Shibanping landslide (Wang, 2023; Gao et al., 2025).

Rock/soil mass	State	Unit weight/KN•m ⁻³	Internal friction angle/°	Cohesion/MPa Poisson's ratio	Poisson's ratio	Elastic modulus/GPa	Porosity	Permeability coefffcient/cm x s ⁻¹
	Nature	24.8	37	5.02	0.20	5.19	ī.	£10.5
Argulaceous sandstone	Saturation	24.9	35	4.65	0.23	3.90	0.51	- 10
	Nature	20.2	16	0.0155	0.30	0.21	Ç	
Arginized interiayer	Saturation	20.6	12	0.0109	0.31	0.20	0.43	10
-	Nature	24.7	50	8.08	0.19	6.31	Č	2 - 0 -
Sandstone	Saturation	24.8	47	7.90	0.21	5.54	0.52	- 01

TABLE 2 Stability calculation results of the Shibanping landslide under different methods.

State	Stability coefficient				
	Plane sliding method	Numerical simulation method			
Nature	1.37	1.36			
Rainfall	0.99	1.03			
Earthquake	1.12	1.15			



4.3 Verification and comparative analysis

To verify the reliability of the conclusions from the numerical simulation and simplified limit equilibrium analysis, this study conducted a combined displacement-seepage observation of the Shibanping landslide during rainfall and performed a comparative analysis with the model results. The monitoring layout includes: GNSS reference points L1–L3 (with a sampling interval of 1 h) and pore water pressure gauges P1–P2. This section presents representative comparative results within the 60-h heavy rainfall duration (Table 3).

Under natural conditions, the cumulative displacement rate of GNSS is less than 0.5 mm/month, the pore water pressure remains basically stable, and the annual average deformation measured by InSAR during the monitoring period is at the millimeter per year level. Overall, these observations are consistent with the conclusion that "the factor of safety (F_S) is 1.36–1.37 under natural working conditions".

The cumulative rainfall during this rainfall event was approximately 168 mm over 60 h. The observations are consistent with the simulations (Table 3): Evolution of the Factor of Safety (F_S): The F_S decreased from 1.36 (at 12 h) \Rightarrow 1.22 (at 24 h) \Rightarrow 1.12 (at 36 h) \Rightarrow 1.05 (at 48 h) \Rightarrow 1.03 (at 60 h). The decrease was significant in the first 48 h of rainfall, and entered a slow-changing phase from 48 h to 60 h.

GNSS Displacement Response (taking L2 as an example): The cumulative displacement was 4 mm (at 12 h) \rightarrow 10 mm (at 24 h) \rightarrow 18 mm (at 36 h) \rightarrow 26 mm (at 48 h) \rightarrow 29 mm (at 60 h). An acceleration phase occurred between 36 h and 48 h, which was synchronized with the phase of rapid decline in the Factor of Safety (F_S).

The pore water pressure at P1 increased by approximately 8, 14, 19, 22, and 23 kPa relative to the initial value (corresponding to 12, 24, 36, 48, and 60 h), and the groundwater level rose by \sim 2.1 m. This is consistent with the evolution of the seepage field in the model.

When the Factor of Safety (F_S) approaches 1.05–1.03, the FS curve shifts from a "rapid decline" phase to a "slow change" phase, and the GNSS displacement curve synchronously transitions from an "acceleration phase" to a "deceleration–stabilization phase. This can serve as an on-site indicator for the boundary between "critical stability" and "basic stability".

During the monitoring period, no strong ground motion corresponding to the model's "critical reduction coefficient of 1.15" was recorded. GNSS only captured small-scale transient disturbances (less than 3 mm per event), which were below the

TABLE 3 Comparison between model results and monitor observations.

State	Simulation result (F_S)	GNSS displacement (L2, cumulative)	Pore water pressure and groundwater response		Consistency identification
		cumulative	P1	P2	
Nature	1.36–1.37	<0.5 mm	Basically unchanged	Basically unchanged	Stable, match
Rainfall 12 h	1.36	4.0 mm	+8 kPa, water level + 0.8 m	+6 kPa, water level + 0.8 m	Match
Rainfall 24 h	1.22	10.0 mm	+14 kPa, water level + 1.3 m	+11 kPa, water level + 1.3 m	Match
Rainfall 36 h	1.12	18.0 mm	+19 kPa, water level +	+16 kPa, water level +	Match
Rainfall 48 h	1.05	26.0 mm	+22 kPa, water level + 2.0 m	+19 kPa, water level + 2.0 m	Match
Rainfall 60 h	1.03	29.0 mm	+23 kPa, water level + 2.1 m	+20 kPa, water level + 2.1 m	Match
Earthquake	≥1.15	<3 mm (transient)	_	_	Match

model's trigger threshold. Therefore, a one-to-one comparison equivalent to that for strong earthquakes cannot be provided temporarily. We have supplemented explanations in the "Discussion and Limitations" section: the current verification focuses on rainfall-induced stability evolution, and the on-site verification of seismic working conditions will be improved with the supplementation of subsequent monitoring data.

5 Discussion

Rainfall and earthquakes are among the most common factors affecting landslide instability; however, their characteristics of influencing the landslide instability process differ. For rainfall, in addition to increasing the self-weight of the soil mass itself, the impact of the rainfall infiltration process on the landslide's rock-soil mass must also be considered. This is closely related to the type of rock-soil mass, degree of weathering, slope angle, and sliding surface depth. Under different rainfall durations, the saturation degree of the landslide's rock-soil mass varies, leading to differences in the induced pore water pressure and, ultimately, differences in displacement. Therefore, this chapter will first analyze the impact of rainfall on the landslide instability process from the perspectives of saturation degree, pore water pressure, and displacement. Changes in the displacement field are closely associated with the overall instability of the landslide. Whether under the action of rainfall or earthquakes, the deformation and failure of a landslide are ultimately manifested through the occurrence of deformation. Next, the characteristics of landslide displacement changes under seismic conditions will be discussed. Finally, by comprehensively considering the deformation and failure characteristics, influencing factors, mechanism, and stability of the landslide, this chapter will explore its prevention and control measures, thereby providing useful references for land management.

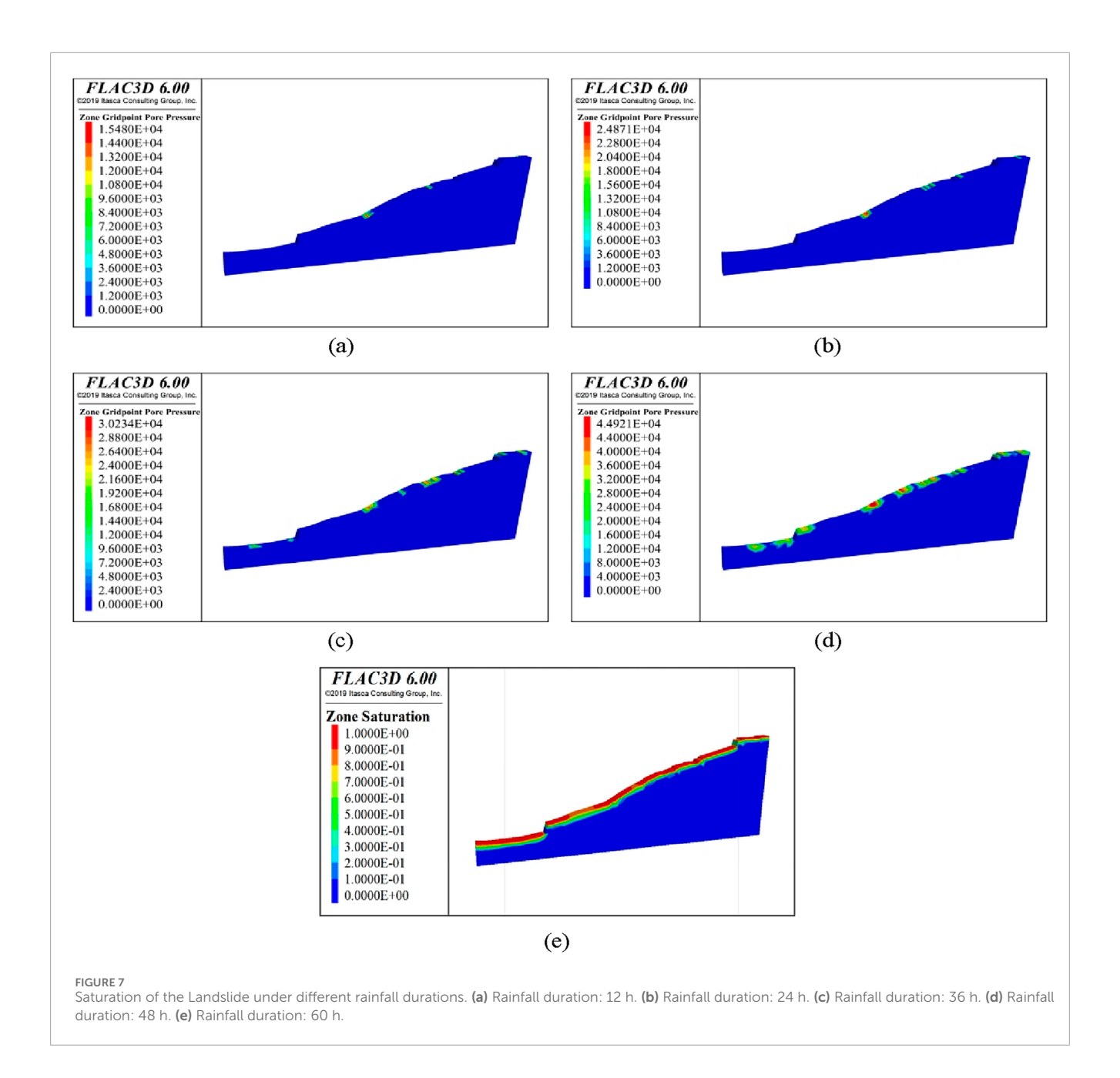
5.1 Impact of rainfall on landslide instability

Saturation degree is a crucial parameter describing the extent of pore water filling in rock masses. It is typically used to represent the ratio of the volume of water in rock pores to the total pore volume. The magnitude of saturation degree directly affects the mechanical properties of rock masses, particularly their shear strength, deformation characteristics, and stability under external loads such as rainfall. Therefore, studying the impact of changes in rock mass saturation degree during rainfall on landslide stability is of great importance.

As shown in Figure 7, with the continuous progression of rainfall, rainwater gradually infiltrates and fills the pores of the rock mass, leading to a steady increase in the rock mass's saturation degree. This process indicates that rainfall, through continuous water infiltration, gradually alters the moisture state of the rock mass, thereby influencing its mechanical properties. Rainwater infiltration is not limited to the surface layer of the rock mass; instead, it gradually extends to deeper layers, causing pores in more areas to be occupied by water. As rainfall duration increases, the infiltration depth gradually increases, and the range of saturation degree expansion also continues to extend—resulting in significant changes to the hydraulic state of the entire rock mass.

When the rainfall duration reaches 60 h, the slope surface area of the landslide is close to a saturated state. This phenomenon indicates that under continuous rainfall, the pore water filling in the rock mass gradually reaches the maximum saturation level. At this point, the effective stress of the rock mass decreases significantly. Especially in rock formations such as weak interlayers and argillaceous sandstones, the increase in saturation degree may lead to a sharp reduction in shear strength in these areas, thereby increasing the probability of landslide occurrence.

Pore water pressure refers to the pressure exerted by the water within the pores of the rock mass. It plays a crucial role in the



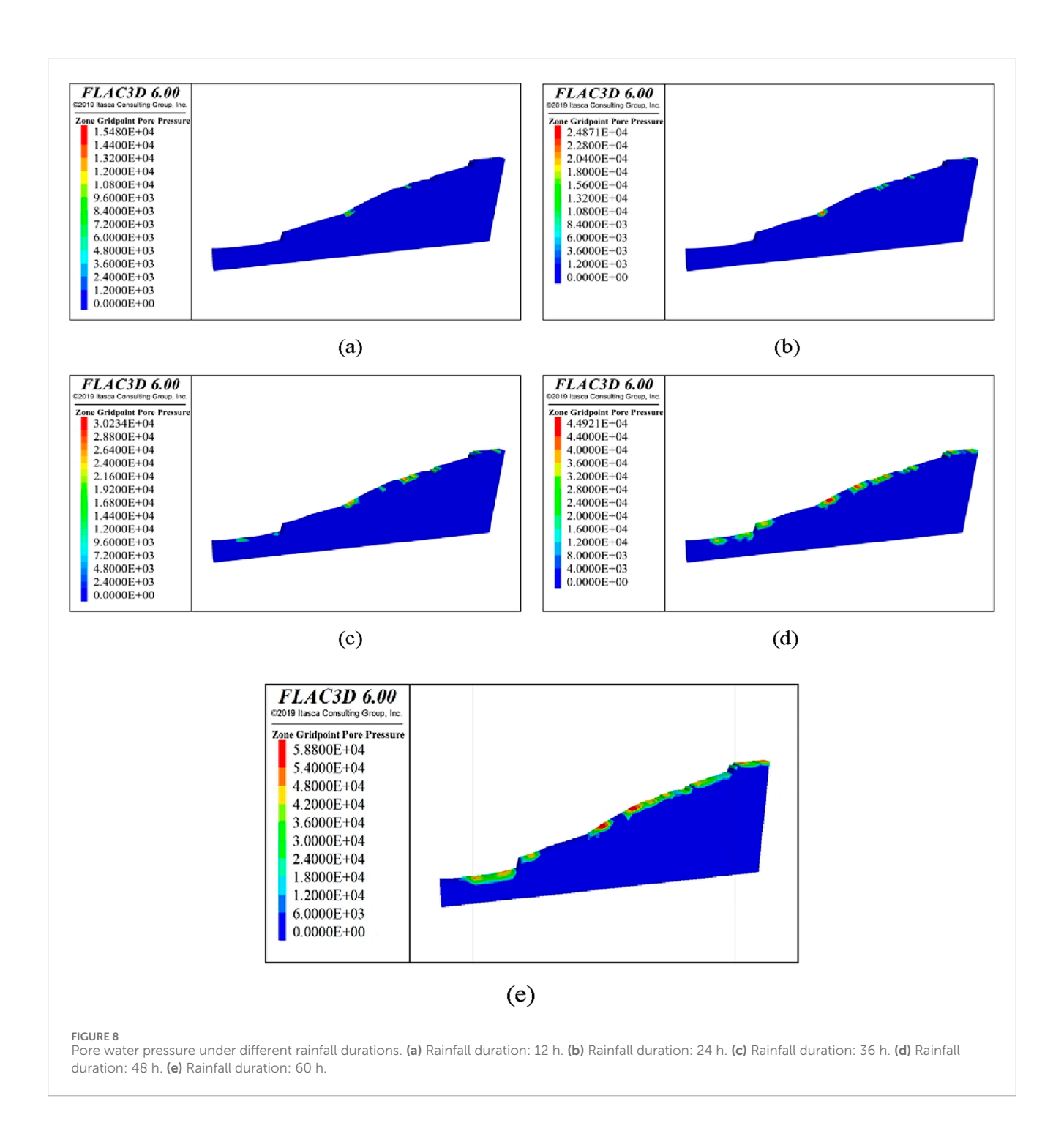
mechanical behavior of the rock mass. Changes in pore water pressure directly affect the effective stress, shear strength, and stability of the rock mass. Specifically, an increase in pore water pressure reduces the effective stress of the rock mass, which in turn weakens its shear strength and makes it more susceptible to deformation or sliding. Understanding the role of pore water pressure in the landslide process is essential for evaluating landslide stability and its triggering mechanisms.

As shown in Figure 8, as the rainfall progresses, rainwater gradually infiltrates into the rock mass, leading to a gradual increase in pore water pressure. During this process, the pore water pressure rises from an initial value of 1.54×10^3 kPa to 5.88×10^3 kPa, indicating that rainfall significantly increases the pore water pressure inside the rock mass. The increase in pore water pressure leads to a decrease in the effective stress of the rock mass, thereby reducing

its shear strength, especially in weak interlayers or mudstone layers, where this effect is particularly pronounced.

From 36 to 48 h of rainfall, the pore water pressure showed significant changes, especially in the mudstone layer at the base of the slope. The infiltration of rainwater caused the pore water pressure at the slope base to rise rapidly, thus affecting the stability of the area. Given that mudstone has relatively high permeability, water infiltrating through this layer not only increases the pore water pressure but could also trigger deformation and sliding of the landslide body.

This phenomenon underscores the crucial role of rainfall in triggering landslides, especially the direct impact of pore water pressure on rock mass stability. As rainfall continues, the further increase in pore water pressure may lead to a continuous reduction in effective stress, thereby increasing the risk of landslide occurrence.

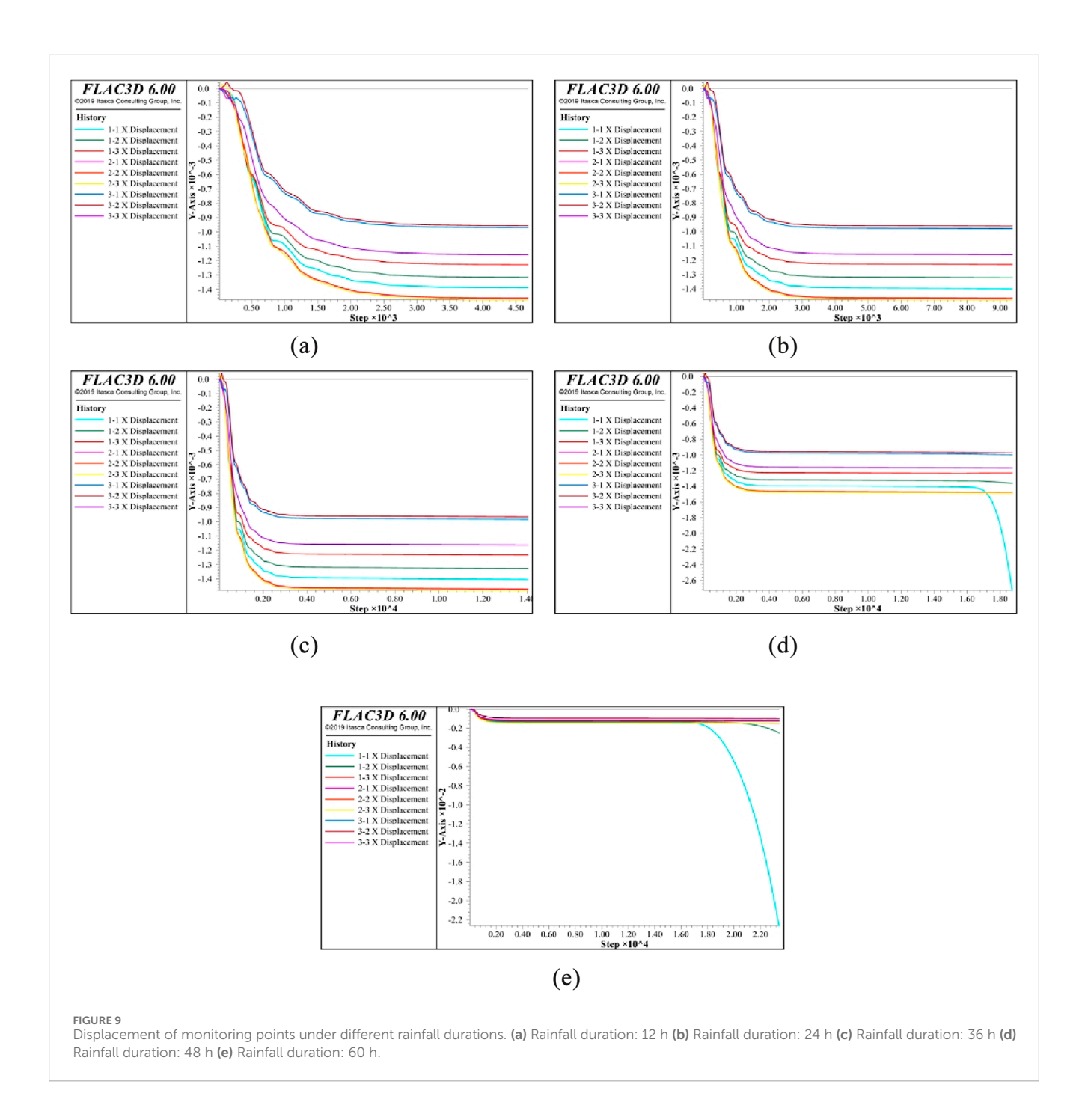


Therefore, accurately assessing the variation of pore water pressure during rainfall and its impact on landslide stability is vital for landslide hazard prediction and prevention.

In the process of simulating rainfall's impact on landslides, considering the presence of argillized interlayers in the landslide, multiple monitoring sections and monitoring points were set up to study the variation law of landslide displacement under different rainfall durations. As shown in Figure 9, when the rainfall duration was 12 h, 24 h, and 36 h, the displacement of each monitoring point on the landslide showed almost no change. This indicates that under short-term rainfall, the landslide mass did not undergo

significant deformation or sliding. However, with the increase in rainfall duration—especially when the rainfall duration reached 48 hours—the displacement of Monitoring Point 1-1 began to increase significantly. This change suggests that as rainfall persisted, the rock mass above the argillized interlayer started to be affected, and initial deformation appeared at the slope toe. The occurrence of this phenomenon implies that rainfall not only affected the pore pressure of the rock mass hydraulically but also may have caused stress redistribution inside the rock mass.

When the rainfall duration further increased to 60 h, the displacement of Monitoring Points 1-1 and 1-2 increased

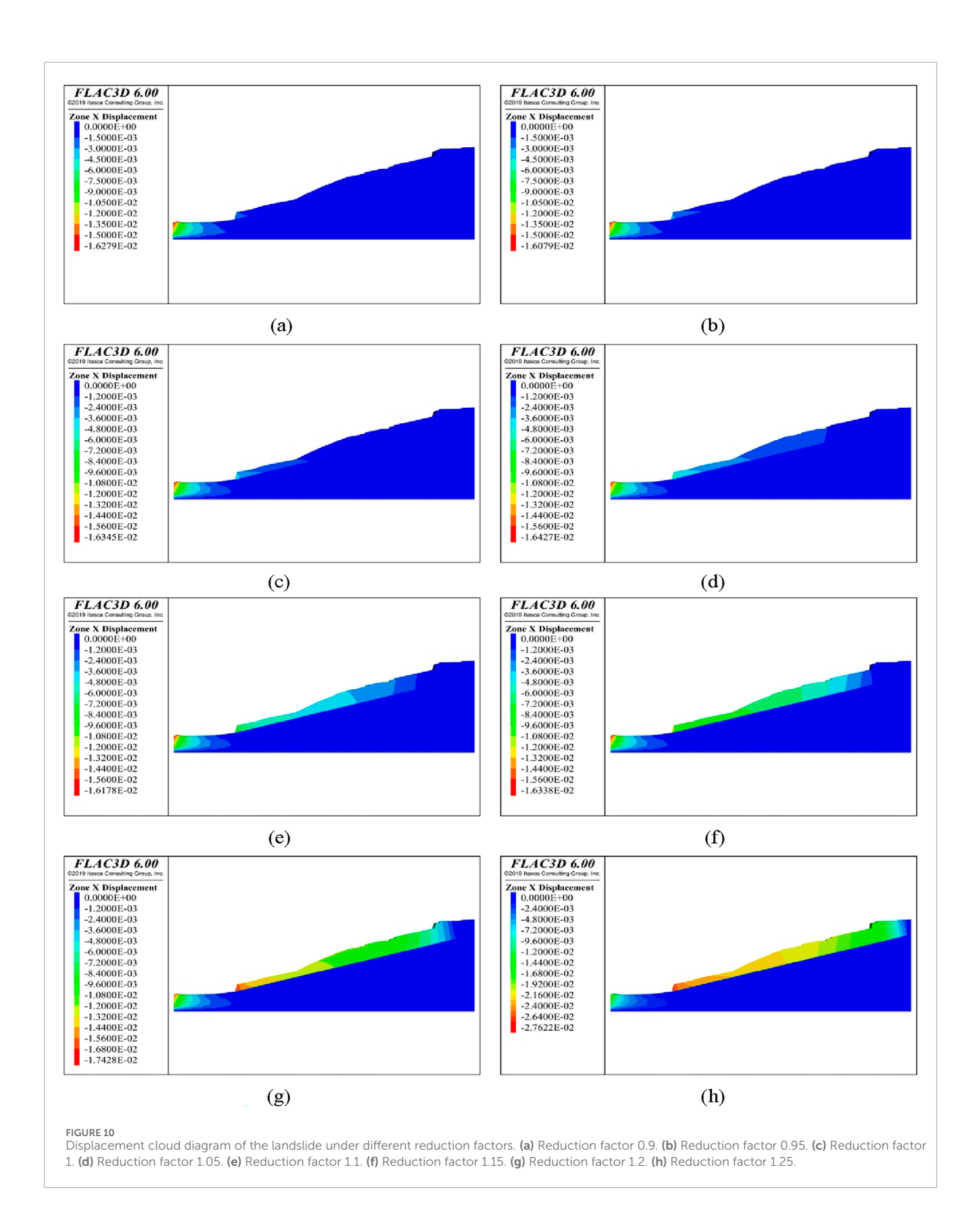


significantly, which further confirmed the gradual instability trend of the rock mass. Specifically, the water infiltration caused by rainfall reduced the shear strength of the argillized interlayer, thereby promoting the sliding of the rock mass above the structural plane and ultimately leading to the sliding of the landslide. The significant increase in displacement of Monitoring Points 1-1 and 1-2 reflects the gradual expansion of the landslide mass, and this deformation exhibits a progressive instability mode from local to overall.

A comprehensive analysis indicates that during the continuous rainfall process, the Shibanping landslide underwent a sequence of "infiltration \rightarrow suction attenuation/pore pressure rise \rightarrow rapid decline in Factor of Safety $(F_{\rm S})$ \rightarrow accelerated displacement". The FS value

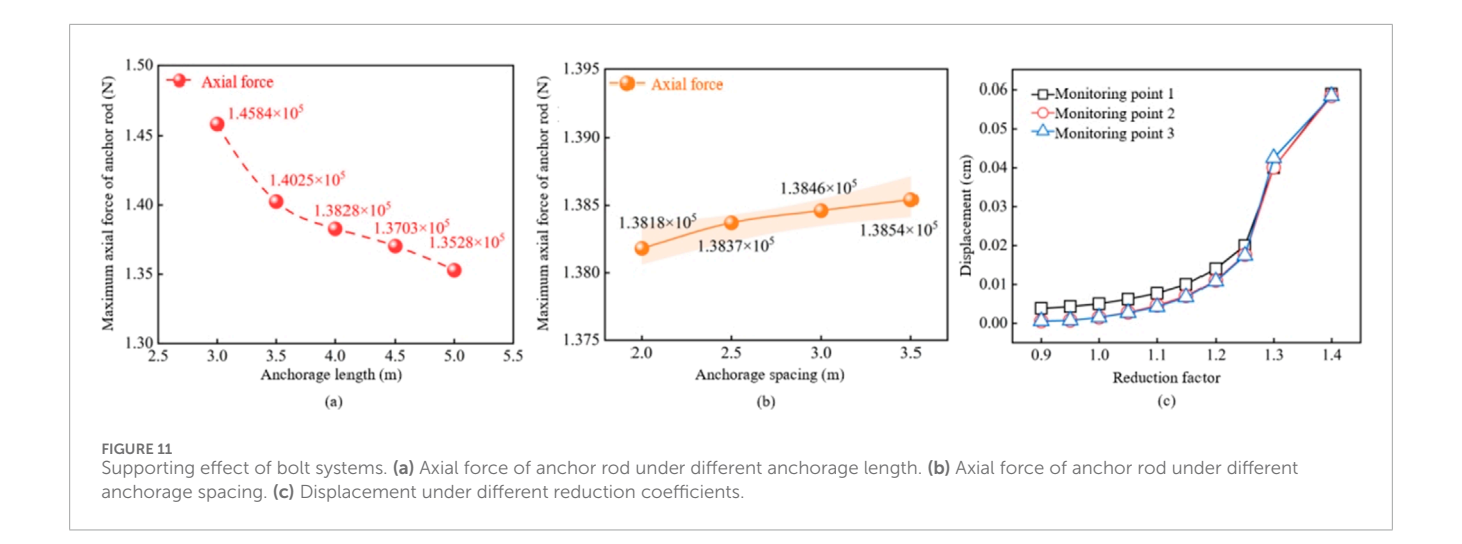
changed over time as follows: 1.36 (at 12 h) \Rightarrow 1.22 (at 24 h) \Rightarrow 1.12 (at 36 h) \Rightarrow 1.05 (at 48 h) \Rightarrow 1.03 (at 60 h). The cumulative displacement of GNSS (L2) was $4 \Rightarrow 10 \Rightarrow 18 \Rightarrow 26 \Rightarrow 29$ mm, with a significant acceleration phase occurring between 36 h and 48 h. The pore water pressure increased by approximately $+8 \Rightarrow +14 \Rightarrow +19 \Rightarrow +22 \Rightarrow +23$ kPa relative to the initial value, and the groundwater level rose by \sim 2.1 m.

The research results are consistent with Iverson's infiltration-triggered model based on the reduced form of the Richards equation, as well as Lu & Godt's stability framework for variably saturated effective stress. Under continuous infiltration, the reduction in effective stress leads to the attenuation of shear strength, which



in turn results in time-series characteristics of "acceleration → critical state → quasi-steady state" (Iverson, 2000; Lu and Godt, 2013). From a threshold perspective, (Bogaard and Greco.,

2016; Bogaard and Greco., 2018) proposed replacing the simple I–D (Intensity–Duration) threshold with a hydro-meteorological threshold to reflect the "cross-threshold process" of the slope's



hydrological response. The acceleration window identified in this study between 36 h and 48 h is consistent with this theory (Bogaard and Greco, 2016; 2018).

The "threshold crossing \Rightarrow rapid strength attenuation \Rightarrow quasisteady plateau (FS \approx 1.03)" process-based response exhibited by the Shibanping landslide under rainfall is also consistent with the dominant understanding of international physical infiltration models and threshold methods (Iverson, 2000).

This phenomenon indicates that the instability of the landslide is a progressive process. In the initial stage, it is mainly manifested as local deformation; however, as the rainfall duration extends, the deformation gradually expands to the entire landslide mass. Through a systematic analysis of landslide displacement under different rainfall durations, the gradual evolution process of the landslide from local instability to overall failure can be clearly observed. The emergence of this progressive instability mode provides an important basis for the early warning of landslides and also offers scientific support for the formulation of landslide prevention and control strategies.

5.2 Impact of earthquake on landslide instability

According to Figure 10, when the reduction coefficient increases to 1.15, the region of maximum displacement of the landslide undergoes a significant change, becoming completely concentrated in the rock mass area above the argillized interlayer. This phenomenon indicates that as the reduction coefficient increases, the role of the argillized interlayer in the landslide becomes increasingly prominent, making it a key factor affecting landslide stability.

Specifically, the reduction coefficient reflects changes in the strength of the rock mass. As this coefficient increases, the shear strength of the rock mass gradually decreases, leading to a decline in landslide stability. Analysis of the displacement field reveals that when the reduction coefficient is small, the displacement distribution of the landslide is relatively uniform, with no obvious strain concentration observed in local areas. However, when the reduction coefficient reaches 1.15, the maximum displacement of

the landslide begins to concentrate significantly in the argillized interlayer region—indicating that the weak structural plane in this region plays a dominant role in the occurrence of the landslide. This result is highly consistent with the Newmark–Jibson framework: permanent displacement occurs and concentrates along weak layers only when the equivalent (or actual) acceleration exceeds the yield/critical acceleration; if the threshold is not reached, only a recoverable transient response is exhibited. Multiple studies on the 2013 Lushan Earthquake and 2022 Luding Earthquake in China also indicate that the combination of "strong earthquake and weak layer" is a key condition for the concentration of landslide displacement and the expansion of its scale (Jibson, 2007).

Due to its low strength and high deformability, the argillized interlayer serves as the weak link in landslide occurrence. Under the action of external factors such as earthquakes and rainfall, the rock mass in this interlayer region gradually loses stability, ultimately leading to the occurrence of landslides. Therefore, the concentration of displacement in the rock mass above the argillized interlayer highlights the critical role of this layer in the landslide instability process. This phenomenon not only reveals the close relationship between the reduction coefficient and landslide stability but also emphasizes the argillized interlayer as a triggering factor for landslide instability.

5.3 Support countermeasures analysis

The anchorage support system is an engineering technology that forms a composite structure by interacting with rock-soil masses through rock bolts or anchor cables, thereby enhancing the stability of slopes or rock-soil masses. Meanwhile, rock bolt support can penetrate weak interlayers and extend 3–8 meters into stable rock formations, effectively controlling shear failure along the weak interlayers. Additionally, rock bolt support does not require large-scale excavation, causing minimal damage to the original stress field of the slope. Furthermore, the length of rock bolts and anchorage spacing can be adjusted according to stratum conditions, making it adaptable to different weathering degrees and fracture development situations.

Therefore, we simulated the mechanical performance of anchorage under different anchorage lengths and anchorage spacings, as well as the stability of the landslide under the combined action of rainfall and earthquake under the optimal anchorage parameters (Figure 11). According to Figure 11a,b, the larger the anchorage length, the continuous decrease in the axial force of the rock bolt; as the anchorage spacing increases, the axial force of a single rock bolt increases. According to Figure 11c, when the reduction coefficient reaches 1.25, the horizontal displacement shows a sharp upward trend. It can be considered that the stability coefficient after reinforcement is 1.25, which is significantly higher than the 1.15 of the unreinforced state. For this reason, it can be concluded that "drainage + anchorage support" is applicable to the prevention and control of this landslide.

6 Conclusion

- The occurrence of the Shibanping landslide is closely related to factors such as rainfall, lithology, excavation, topography and geomorphology, and geological structures. The relatively steep terrain slope and the heterogeneous structure of the rock mass provide favorable conditions for the formation of the landslide. In particular, the argillized interlayer significantly reduces the shear strength under the action of rainfall and earthquakes, which promotes the occurrence of the landslide.
- 2. The deformation of the landslide starts with tension cracking and downward displacement at the top. Under the action of rainfall and excavation, it gradually expands to deeper layers and the leading edge. Particularly on the sliding surface of the argillized interlayer, the deformation and failure gradually deepen and spread, eventually leading to the collapse of the leading edge and the formation of the landslide. Its mechanism is progressive-bedding slip.
- 3. Rainfall exacerbates landslide instability by increasing the self-weight, saturation degree, and pore water pressure of the landslide's rock-soil mass, which in turn leads to a continuous decrease in effective stress. Earthquakes reduce slope stability through shear stress induced by seismic waves. Particularly in areas with weak structural planes, the combined effect of rainfall and earthquakes makes the instability process of the landslide mass more complex and intense.

Data availability statement

The raw data supporting the conclusions of this article will be made available by the authors, without undue reservation.

Author contributions

LW: Funding acquisition, Writing – original draft. WG: Writing – review and editing. SB: Writing – original draft. RB: Writing –

original draft. LZ: Funding acquisition, Writing – original draft. ZH: Funding acquisition, Writing – original draft. BH: Writing – review and editing. FC: Funding acquisition, Writing – original draft. JJ: Writing – original draft. MG: Funding acquisition, Writing – original draft.

Funding

The authors declare that financial support was received for the research and/or publication of this article. This research was supported by Humanities and Social Sciences Youth Foundation, Ministry of Education (23YJCZH051), the Opening Foundation of Key Laboratory of Landslide Risk Early-warning and Control, Ministry of Emergency Management (Chengdu University of Technology) (KLLREC2022K003), the Opening Foundation of State Key Laboratory of Geological Hazard Prevention and Geoenvironmental Protection (SKLGP2024K007), the Opening Foundation of Major Hazard Measurement and Control Key Laboratory of Sichuan Province (KFKT2023-04), Natural Science Foundation of Sichuan Province (2024YFFK0111, 2024NSFSC0971) and Sichuan Provincial 'Bidding for Talents' Project (2025YFNH0008).

Conflict of interest

Author JJ was employed by Chongqing 208 Geological Environment Research Institute Co., Ltd.

The remaining authors declare that the research was conducted in the absence of any commercial or financial relationships that could be construed as a potential conflict of interest.

Generative AI statement

The authors declare that no Generative AI was used in the creation of this manuscript.

Any alternative text (alt text) provided alongside figures in this article has been generated by Frontiers with the support of artificial intelligence and reasonable efforts have been made to ensure accuracy, including review by the authors wherever possible. If you identify any issues, please contact us.

Publisher's note

All claims expressed in this article are solely those of the authors and do not necessarily represent those of their affiliated organizations, or those of the publisher, the editors and the reviewers. Any product that may be evaluated in this article, or claim that may be made by its manufacturer, is not guaranteed or endorsed by the publisher.

References

Bogaard, T., and Greco, R. (2016). Landslide hydrology: from hydrology to pore pressure. WIREs Water 3 (3), 439–459. doi:10.1002/wat2.1126

Bogaard, T., and Greco, R. (2018). Invited perspectives: hydrological perspectives on precipitation intensity-duration thresholds for landslide initiation: proposing hydrometeorological thresholds. *Nat. Hazards Earth Syst. Sci.* 18, 31–39. doi:10.5194/nhess-18-31-2018

Cemiloglu, A., Zhu, L., Mohammednour, A. B., Azarafza, M., and Nanehkaran, Y. A. (2023). Landslide susceptibility assessment for Maragheh county, Iran, using the logistic regression algorithm. *Land* 12 (7), 1397. doi:10.3390/land12071397

Chen, Y., Song, C., Li, Z. H., Yu, C., Liu, Z. J., Zhang, X. S., et al. (2024). Characterizing the evolution of the Daguangbao landslide nearly 15 years after the 2008 Wenchuan earthquake by InSAR observations. *Eng. Geol.* 342, 107748. doi:10.1016/J.ENGGEO.2024.107748

Gao, M. B., He, B. B., Li, W. H., Guo, W. J., Bai, S. M., Wang, L. J., et al. (2025). Study on mechanical properties of rock and soil mass in the slip zone of shibanping landslide. Front. Earth Sci. 13, 1675192. doi:10.3389/feart.2025.1675192

He, S., Shen, F., Chen, T., Mitri, H., Ren, T., and Song, D. (2023). Study on the seismic damage and dynamic support of roadway surrounding rock based on reconstructive transverse and longitudinal waves. *Adv. Geo-Energy Res.* 9 (3), 156–171. doi:10.46690/ager.2023.09.04

Iverson, R. M. (2000). Landslide triggering by rain infiltration. Water Resour. Res. 36 (7), 1897–1910. doi:10.1029/2000wr900090

Jibson, R. W. (2007). Regression models for estimating coseismic landslide displacement. *Eng. Geol.* 91, 209–218. doi:10.1016/j.enggeo.2007.01.013

Khan, M. I., and Wang, S. (2021). Slope stability analysis to correlate shear strength with slope angle and shear stress by considering saturated and unsaturated seismic conditions. *Appl. Sci.* 11 (10), 4568. doi:10.3390/APP11104568

Kurlenya, M. V., Chernyshov, G. S., Serdyukov, A. S., Duchkov, A. A., and Yablokov, A. V. (2016). Procedure and results of seismic investigations into causes of landslides in permafrost rocks. *J. Min. Sci.* 52, 835–841. doi:10.1134/S1062739116041273

Li, Z. B., Yin, C., Tan, Z. Y., Liu, X. L., Li, S. F., and Zhang, X. X. (2023). Rainfall-seismic coupling effect induced landslide hazard assessment. *Nat. Hazards* 118 (3), 2123–2152. doi:10.1007/S11069-023-06084-W

Lu, N., and Godt, J. W. (2013). Hillslope hydrology and stability. Cambridge University Press. doi:10.1017/CBO9781139108164

Ma, S., Shao, X. Y., Xu, C., Chen, X. L., and Yuan, R. M. (2025). Topographic location and connectivity to channel of earthquake-and rainfall-induced landslides in loess Plateau area. *Sci. Rep.* 15 (1), 628. doi:10.1038/S41598-024-84885-0

Mao, Y. M., Chen, L., Nanehkaran, Y. A., Azarafza, M., and Derakhshani, R. (2023). Fuzzy-based intelligent model for rapid rock slope stability analysis using q_{slope} . *Water* 15 (16), 2949. doi:10.3390/w15162949

Marotti, J. C., Gomes, G. J. C., Velloso, R. Q., Vargas junior, E. A., Nunes, R. S., and Fernandes, N. F. (2023). Exploring extreme rainfall-triggered landslides using 3D unsaturated flow antecedent moisture and spatially distributed soil depth. *Catena* 229, 107241. doi:10.1016/J.CATENA.2023.107241

Marui, H., and Wanfg, C. X. (2015). Earthquake-induced landslides: an overview. Eng. Geol. Soc. Territ. 2, 713–715. doi:10.1007/978-3-319-09057-3_119

Montgomery, D. R., and Dietrich, W. E. (1994). A physically based model for the topographic control on shallow landsliding. *Water Resour. Res.* 30 (4), 1153–1171. doi:10.1029/93WR02979

Montoya-Araque, E. A., Montoya-Noguera, S., Lopez-Caballero, F., and Gatti, F. (2025). Numerical earthquake-induced landslide hazard assessment at regional scale in the Colombian andes. *Soil Dyn. Earthq. Eng.* 195, 109370. doi:10.1016/J.SOILDYN.2025.109370

Moska, R., Labus, K., and Kasza, P. (2024). Dynamic elastic properties, petrophysical parameters and brittleness of hot dry rocks from prospective areas of central Europe. *Adv. Geo-Energy Res.* 14 (2), 90–105. doi:10.46690/ager.2024.11.03

Nandi, S., and Ghosh, P. (2025). Probabilistic seismic slope stability analysis adopting limiting profile approach. $Eng.\ Geol.\ 354,\ 108174.\ doi:10.1016/J.ENGGEO.2025.108174$

Nanehkaran, Y. A., Mao, Y., Azarafza, M., Kockar, M. K., and Zhu, H. H. (2021). Fuzzy-based multiple decision method for landslide susceptibility and hazard assessment: a case study of tabriz, Iran. *Geomechanics Eng.* 24 (5), 407–418. doi:10.12989/GAE.2021.24.5.407

Nanehkaran, Y. A., Licai, Z., Chen, J., Mao, Y. M., and Yimin, M. (2022). Application of artificial neural networks and geographic information system to provide hazard susceptibility maps for rockfall failures. *Environ. Earth Sci.* 81, 475. doi:10.1007/s12665-022-10603-6

Nanehkaran, Y. A., Licai, Z., Chengyong, J., Chen, J., Anwar, S., Azarafza, M., et al. (2023). Comparative analysis for slope stability by using machine learning methods. *Appl. Sci.* 13 (3), 1555. doi:10.3390/app13031555

Qiu, L., Zhu, Y., Liu, Q., Guo, M., Song, D., and Wang, A. (2023). Response law and indicator selection of seismic wave velocity for coal seam outburst risk. *Adv. Geo-Energy Res.* 9 (3), 198–210. doi:10.46690/ager.2023.09.07

Rajaram, C., Vemuri, J., and Akansel, V. H. (2025). Near-field ground motion intensity parameters of the major February 06, 2023, Türkey Kahramanmaraş earthquake sequences. *Geohazard Mech.* 3 (3), 177–186. doi:10.1016/j.ghm.2025.08.002

Ren, J., Sun, P., Zhang, S., Li, R. J., Wang, H. J., and Zhang, J. (2023). Experimental study on the failure mechanism of the zhoujiashan landslide under the combined effect of rainfall and earthquake in tianshui city, northwest China. *Bull. Eng. Geol. Environ.* 82 (12), 436. doi:10.1007/S10064-023-03464-1

Sassa, K., Matsunami, K., Doan, L., Miyagi, T., Thaldena, N., Weerasinghe, R., et al. (2023). The 2023.4. 24 hambantota-offshore earthquake and microearthquakes in Sri Lanka and the landslide risk evaluation in a nearby slope by post-rainfall earthquakes. *Landslides* 20 (4), 1771–1779. doi:10.1007/s10346-023-02108-5

Shu, H. P., He, J. L., Zhang, F. Y., Ma, J., Chen, Y., Yang, S. J., et al. (2024). Construction of landslide warning by combining rainfall threshold and landslide susceptibility in the gully region of the loess Plateau: a case of lanzhou city, China. *J. Hydrology* 645, 132148. doi:10.1016/J.JHYDROL.2024.132148

Song, C., Chen, B., Li, Y., Li, Z. H., Du, J. T., Yu, C., et al. (2025). Amplified coseismic loess failure and postseismic landslide acceleration triggered by the 2023 Jishishan, China earthquake. *Eng. Geol.* 352, 108074. doi:10.1016/j.enggeo.2025.108074

Tang, C. J., and Marshall, A. M. (2025). Ground collapse: effect of building position on tunnelling-induced soil movements. *Geohazard Mech.* 3 (3), 165–176. doi:10.1016/j.ghm.2025.08.001

Wang, S. Y. (2023). Study on the stability of bedding slope of soil-rock composite stratum. Nanjing: Southeast University. doi:10.27014/d.cnki.gdnau.2023.002198

Wang, C., Li, T. H., Hu, S., and Hu, B. (2025). Seismic stability analysis of Shiliushubao old landslide considering the spatial distribution of dynamic parameters after heavy rainfall. *Bull. Eng. Geol. Environ.* 84 (7), 367–15. doi:10.1007/S10064-025-04373-1

Wu, Y. Z., Dong, Y. D., Wei, Z. X., Dong, J. H., Peng, L., Yan, P., et al. (2023). Genetic mechanisms and a stability evaluation of large landslides in Zhangjiawan, Qinghai province. *Front. Earth Sci.* 11, 1140030. doi:10.3389/FEART.2023.1140030

Zhao, B. R., Marin, R. J., Luo, W., Yu, Z. Y., and Yuan, L. W. (2025). Rainfall thresholds for shallow landslides considering rainfall temporal patterns. *Bull. Eng. Geol. Environ.* 84 (3), 132–13. doi:10.1007/S10064-025-04144-Y

Zhu, S. B., Shi, Y. L., Lu, M., and Xie, F. R. (2013). Dynamic mechanisms of earthquake triggered landslides. *Sci. China Earth Sci.* 56 (10), 1769–1779. doi:10.1007/s11430-013-4582-9